# GEOPHYSICS

## P-SV wave propagation in heterogeneous media: Velocity-stress finite-difference method

Jean Virieux*

### ABSTRACT

I present a finite-difference method for modeling P-SV wave propagation in heterogeneous media. This is an extension of the method I previously proposed for modeling SH-wave propagation by using velocity and stress in a discrete grid. The two components of the velocity cannot be defined at the same node for a complete staggered grid: the stability condition and the P-wave phase velocity dispersion curve do not depend on the Poisson's ratio, while the S-wave phase velocity dispersion curve behavior is rather insensitive to the Poisson's ratio. Therefore, the same code used for elastic media can be used for liquid media, where S-wave ve-

locity goes to zero, and no special treatment is needed for a liquid-solid interface. Typical physical phenomena arising with P-SV modeling, such as surface waves, are in agreement with analytical results. The weathered-layer and corner-edge models show in seismograms the same converted phases obtained by previous authors. This method gives stable results for step discontinuities, as shown for a liquid layer above an elastic half-space. The head wave preserves the correct amplitude. Finally, the corner-edge model illustrates a more complex geometry for the liquid-solid interface. As the Poisson's ratio $\nu$ increases from 0.25 to 0.5, the shear converted phases are removed from seismograms and from the time section of the wave field.

## INTRODUCTION

Many different methods proposed for modeling waves in heterogeneous media have their own range of validity and interest. Ray theory (Červený et al., 1977), a high-frequency approximation, breaks down in many common situations. At caustics the predicted amplitude is infinite, and in shadow zones the amplitude is zero. Using spectral transformations in space and time, several extensions for overcoming these difficulties have been proposed, depending on how the inverse transformations are performed. Reflectivity (Fuchs and Müller, 1971), which integrates numerically on the slowness vector, is routinely used for vertically heterogeneous media. Numerical integration over wavenumber is used by Aki and Larner (1970) and Bard and Bouchon (1980), who introduced the Rayleigh ansatz for the diffraction sources, in order to model laterally heterogeneous media. More recently, Alekseev

and Mikhailenko (1980) and Mikhailenko and Korneev (1984) performed integration over wavenumber for any interface. Going to the complex slowness plane allows inversion by inspection, giving generalized ray theory (Helmberger, 1968). For computing reflection and refraction coefficients glorified optics (Hong and Helmberger, 1978) introduces two-dimensional (2-D) wave curvature at the interface, while Lee and Langston (1983) took into account two curvatures for a three-dimensional (3-D) wavefront. Chapman (1978) performed the frequency integration before the integration over real slowness, and obtained a WKBJ seismogram which is regular at caustics. By using the Maslov asymptotic transformation, Chapman and Drummond (1982) extended the WKBJ seismogram for laterally inhomogeneous media. Another method called Gaussian beam, which also gives finite results at caustics, is seen as a perturbation of spectral decomposition (Madariaga and Papadimitriou, 1985).

On the other hand, fully numerical techniques in space-time domain, in the finite-difference formulation (Boore, 1972) or finite-element formulation (Smith, 1975), handle any kind of waves in complex media but are limited mainly because numerical dispersion prevents them from propagating waves over large distances. In other words, enough low-frequency waves must be used. Another difficulty that arises with numerical techniques is the interpretation of numerical seismograms. The situation is better than for the real Earth, because the medium is known and fields may be displayed inside the whole medium, thereby defining the shape of wavefronts. Of course, the interpretation becomes more difficult as the complexity of the medium increases.

To model $P$-$SV$ wave propagation, I apply a finite-difference scheme used in Madariaga (1976) for crack propagation modeling. $SH$-wave modeling has already been discussed in a previous article (Virieux, 1984). Here I follow the same formulation of the problem. Numerical analysis is lengthier, because of several interesting features of the $P$-$SV$ scheme. Explosive source and surface waves are compared with analytical results to gain confidence in this modeling. After comparing other numerical simulations with the weathered-layer model and the corner-edge model, I discuss the discrepancy between results obtained for the corner-edge model in the homogeneous and heterogeneous formulations (Kelly et al., 1976). Pictures of the medium display the evolution of wavefronts with respect to time. The liquid-solid interface is studied, and stable results obtained for a liquid layer over an elastic half-space are shown. The case of a complex interface is illustrated by a corner-edge and numerical seismograms for Poisson's ratios $v$ ranging from 0.25 to 0.5 are presented. Pictures of the medium at a given time for different Poisson's ratios help demonstrate its effects on seismograms. For modeling a more complex medium like a salt dome, future work is necessary.

## PROBLEM FORMULATION

I closely follow the development in my previous paper on $SH$-wave propagation (Virieux, 1984). I consider a vertical 2-D medium with a horizontal axis $x$ and a vertical axis $z$ pointing downward. The medium is assumed linearly elastic and isotropic.

### Equations

Instead of using the wave equation which is a second-order hyperbolic system, I go back to the elastodynamic equations which are:

$$\rho \frac{\partial^2 u_x}{\partial t^2} = \frac{\partial \tau_{xx}}{\partial x} + \frac{\partial \tau_{xz}}{\partial z},$$

$$\rho \frac{\partial^2 u_z}{\partial t^2} = \frac{\partial \tau_{xz}}{\partial x} + \frac{\partial \tau_{zz}}{\partial z},$$

$$\tau_{xx} = (\lambda + 2\mu) \frac{\partial u_x}{\partial x} + \lambda \frac{\partial u_z}{\partial z}, \qquad (1)$$

$$\tau_{zz} = (\lambda + 2\mu) \frac{\partial u_z}{\partial z} + \lambda \frac{\partial u_x}{\partial x},$$

and

$$\tau_{xz} = \mu \left( \frac{\partial u_x}{\partial z} + \frac{\partial u_z}{\partial x} \right)$$

In these equations, $(u_x, u_z)$ is the displacement vector and $(\tau_{xx}, \tau_{zz}, \tau_{xz})$ is the stress tensor. $\rho(x, z)$ is the density, and $\lambda(x, z)$ and $\mu(x, z)$ are Lamé coefficients. This system is transformed into the following first-order hyperbolic system:

$$\frac{\partial v_x}{\partial t} = b \left( \frac{\partial \tau_{xx}}{\partial x} + \frac{\partial \tau_{xz}}{\partial z} \right),$$

$$\frac{\partial v_z}{\partial t} = b \left( \frac{\partial \tau_{xz}}{\partial x} + \frac{\partial \tau_{zz}}{\partial z} \right),$$

$$\frac{\partial \tau_{xx}}{\partial t} = (\lambda + 2\mu) \frac{\partial v_x}{\partial x} + \lambda \frac{\partial v_z}{\partial z}, \qquad (2)$$

$$\frac{\partial \tau_{zz}}{\partial t} = (\lambda + 2\mu) \frac{\partial v_z}{\partial z} + \lambda \frac{\partial v_x}{\partial x},$$

and

$$\frac{\partial \tau_{xz}}{\partial t} = \mu \left( \frac{\partial v_x}{\partial z} + \frac{\partial v_z}{\partial x} \right)$$

In these equations $(v_x, v_z)$ is the velocity vector. $b(x, z)$, the lightness or the buoyancy, is the inverse of density.

### Initial conditions

The medium is supposed to be in equilibrium at time $t = 0$, i.e., stress and velocity are set to zero everywhere in the medium. Because of these initial conditions, propagating stress and velocity is also equivalent to propagating "time-integrated stress" and displacement.

### Boundary conditions

Internal interfaces are not treated by explicit boundary conditions because they are in a homogeneous formulation (Kelly et al., 1976). They are represented naturally by changes of elastic parameters and density as they are in a heterogeneous formulation. Only four explicit boundary conditions have to be considered: the four edges of the finite-sized vertical grid. Depending on the problem, different boundary conditions can be used on the edges: approximate-radiation conditions (for simulating an infinite medium), stress-free conditions (also known as the Neumann condition or free-surface condition), or zero-velocity conditions equivalent to zero-displacement conditions (the Dirichlet condition or rigid-surface condition). The radiation conditions are equivalent to the condition B-1 of Clayton and Engquist (1980), and correspond to plane-wave radiation conditions.

### Source excitation

I use an explosive source in this paper. Because, as shown later, stresses $\tau_{xx}$ and $\tau_{zz}$ are defined at the same nodal point, equal incremental amplitudes are added to $\tau_{xx}$ and $\tau_{zz}$ at the point source to simulate a given source excitation. Because $v_x$ and $v_z$ are not computed at the source point, infinite amplitudes are avoided. As shown by Gauthier (1983), this implementation of the source excitation is equivalent to the one

used in Alterman and Karal (1968) for this scheme and it saves computer time. Two source excitations for stress are used: the Gaussian pulse

$$f(t) = e^{-\alpha(t-t_0)^2} \tag{3}$$

for the Lamb's problem with the parameter $\alpha$, which controls the wavelength content of the excitation, equal to 200, and the derivative of a Gaussian pulse for the other models

$$g(t) = -2\alpha(t - t_0)e^{-\alpha(t-t_0)^2} \tag{4}$$

with the parameter $\alpha$ equal to 40. This means that, for a $P$-wave velocity of 6 000 m/s, the $P$-wave half-wavelength is 1 800 m and the $S$-wave half-wavelength is 1 000 m for a Poisson's ratio $\nu = 0.25$. Consequently, a good choice for the grid spacing is around 100 m. $t_0$ is chosen to give a causal signal which is approximately zero for negative time. Throughout this paper, $f(t)$ is written for a Gaussian pulse and $g(t)$ for its derivative.

## NUMERICAL ANALYSIS

Derivatives are discretized by using centered finite-differences. Because the system is a first-order hyperbolic system, the interpolation functions are linear functions (Zienkiewicz and Morgan, 1982, p. 154). Assuming equations are verified at nodes, discretization leads to a unique staggered grid, as shown in Figure 1. The discretization of the medium is the last step in the finite-difference formulation. The major difference from usual schemes is that the different components of the velocity field are not known at the same node. The explicit numerical scheme, equivalent to the system (2), is:

$$U_{i,j}^{k+1/2} = U_{i,j}^{k-1/2} + B_{i,j} \frac{\Delta t}{\Delta x} (\Sigma_{i+1/2,j}^{k} - \Sigma_{i-1/2,j}^{k})$$

$$+ B_{i,j} \frac{\Delta t}{\Delta z} (\Xi_{i,j+1/2}^{k} - \Xi_{i,j-1/2}^{k}),$$

$$V_{i+1/2,j+1/2}^{k+1/2} = V_{i+1/2,j+1/2}^{k-1/2}$$

$$+ B_{i+1/2,j+1/2} \frac{\Delta t}{\Delta x} (\Xi_{i+1,j+1/2}^{k} - \Xi_{i,j+1/2}^{k})$$

$$+ B_{i+1/2,j+1/2} \frac{\Delta t}{\Delta z} (T_{i+1/2,j+1}^{k} - T_{i+1/2,j}^{k}),$$

$$\Sigma_{i+1/2,j}^{k+1} = \Sigma_{i+1/2,j}^{k}$$

$$+ (L + 2M)_{i+1/2,j} \frac{\Delta t}{\Delta x} (U_{i+1,j}^{k+1/2} - U_{i,j}^{k+1/2})$$

$$+ L_{i+1/2,j} \frac{\Delta t}{\Delta z} (V_{i,j+1}^{k+1/2} - V_{i,j}^{k+1/2}),$$

$$T_{i+1/2,j}^{k+1} = T_{i+1/2,j}^{k}$$

$$+ (L + 2M)_{i+1/2,j} \frac{\Delta t}{\Delta z} (V_{i,j+1}^{k+1/2} - V_{i,j}^{k+1/2})$$

$$+ L_{i+1/2,j} \frac{\Delta t}{\Delta x} (U_{i+1,j}^{k+1/2} - U_{i,j}^{k+1/2}),$$

and

$$\Xi_{i,j+1/2}^{k+1} = \Xi_{i,j+1/2}^{k}$$

$$+ M_{i,j+1/2} \frac{\Delta t}{\Delta z} (U_{i,j+1}^{k+1/2} - U_{i,j}^{k+1/2})$$

$$+ M_{i,j+1/2} \frac{\Delta t}{\Delta x} (V_{i+1,j}^{k+1/2} - V_{i,j}^{k+1/2}). \tag{5}$$

In these equations, $k$ is the index for time discretization, $i$ for $x$-axis discretization, and $j$ for $z$-axis discretization. $\Delta t$ is the grid step in time, $\Delta x$ and $\Delta z$ are the grid steps for the $x$-axis and for the $z$-axis, respectively, which are assumed equal in the following applications. Numerical velocity $(U, V) = (v_x, v_z)$ at time $(k + 1/2)\Delta t$, and numerical stress $(\Sigma, \Xi, T) = (\tau_{xx}, \tau_{zz}, \tau_{xz})$ at time $(k + 1)\Delta t$ are computed explicitly from velocity at time $(k - 1/2)\Delta t$ and stress at time $k\Delta t$. $B$ represents the buoyancy inside the medium, while $L$, $M$ represent Lamé coefficients ($\lambda$, $\mu$), as shown in Figure 1.

For homogeneous media, standard spectral analysis gives the following numerical stability condition for this explicit scheme:

$$V_p \Delta t \sqrt{\frac{1}{\Delta x^2} + \frac{1}{\Delta z^2}} < 1, \tag{6}$$

where $V_p$ is the $P$-wave velocity. The stability condition is independent of the $S$-wave velocity $V_s$, or of the Poisson's ratio $\nu$. For the special case $\Delta x = \Delta z$, the stability condition reduces to

$$V_p \frac{\Delta t}{\Delta x} < \frac{1}{\sqrt{2}}. \tag{7}$$

The generalization of this stability condition for an $n$-$D$ space is straightforward and gives the following condition

$$V_p \cdot \Delta t \sqrt{\sum_{i=1}^{n} \frac{1}{\Delta x_i^2}} < 1, \tag{8}$$

and, for $\Delta x_i = \Delta x$,

$$V_p \frac{\Delta t}{\Delta x} = \frac{1}{\sqrt{n}}, \tag{9}$$



● $U$ ; $B$
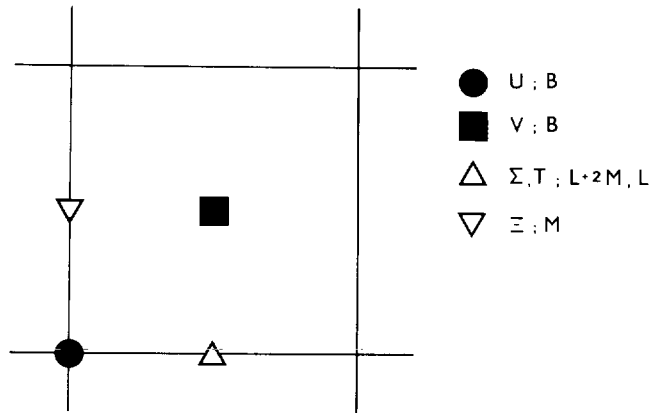■ $V$ ; $B$
△ $\Sigma$, $T$ ; $L + 2M$, $L$
▽ $\Xi$ ; $M$

FIG. 1. Discretization of the medium on a staggered grid. Black symbols are for velocities and buoyancy at time $k\Delta t$. White symbols are for stresses and Lamé coefficients at time $(k + 1/2)\Delta t$.

where $n$ is the dimension of the space. This condition has been verified by Virieux and Madariaga (1982) for 3-D crack modeling. This stability condition is more restrictive than the one obtained for usual finite-difference schemes (Bamberger et al., 1980 or Stephen, 1983) which, for $\Delta x = \Delta z$, gives

$$\sqrt{V_p^2 + V_s^2}\, \frac{\Delta t}{\Delta x} < 1, \tag{10}$$

because the $S$-wave velocity is lower than the $P$-wave velocity. This is the price paid for a complete staggered grid.

Using the same mathematical framework in Bamberger et al., (1980), stability in heterogeneous media is expected provided the condition in equation (6) or (7) holds everywhere on the grid. For the scheme used here, this seems to be true for any Poisson's ratio, as shown later for a liquid-solid interface.

I do not develop the numerical analysis of the finite-difference scheme here because it is lengthy and because it follows standard lines found in many textbooks on numerical analysis (Marchuk, 1975). However I do analyze phase velocity, because it illustrates why a liquid-solid interface is correctly modeled with this finite-difference scheme.

Consider a plane wave with wavenumber $k$, which makes an angle $\theta$ with the $x$-axis. Following Bamberger et al. (1980), the quantity $\gamma$ given by

$$\gamma = \sqrt{2}\, V_p\, \frac{\Delta t}{\Delta x}, \tag{11}$$

controls the numerical dispersion, and the quantity $H$ defined by

## P-WAVE DISPERSION CURVES

## FOR DIFFERENT ANGLES $\vartheta$ AND

## FOR ANY POISSON RATIO $\nu$



FIG. 2. Dispersion curves for nondimensional $P$-wave phase velocity with a dispersion parameter $\gamma = 0.8$. Results for different angles $\theta$ of the plane wave with respect to the $x$-axis are shown. They are independent of Poisson's ratio $\nu$.

$$H = \frac{\Delta x}{\lambda}, \tag{12}$$

controls the number of nodes per wavelength of the plane wave. The resulting nondimensional $P$-wave phase velocity (defined by the ratio of numerical $P$-wave phase velocity to true $P$-wave velocity) is:

$$q_p = \frac{\sqrt{2}}{\pi \gamma H} \sin^{-1}\left[ \frac{\gamma}{\sqrt{2}} \sqrt{\sin^2 (\pi H \cos \theta) + \sin^2 (\pi H \sin \theta)} \right], \tag{13}$$

where $q_p$ is independent of Poisson's ratio $\nu$. Similarly, the nondimensional $S$-wave phase velocity is:

$$q_s = \frac{V_p \sqrt{2}}{V_s \pi \gamma H} \sin^{-1}$$

$$\times \left[ \frac{V_s \gamma}{V_p \sqrt{2}} \sqrt{\sin^2 (\pi H \cos \theta) + \sin^2 (\pi H \sin \theta)} \right], \tag{14}$$

where $q_s$ depends on the Poisson's ratio through $V_s/V_p$. For $\gamma = 0.8$, $q_p(H)$ is shown on Figure 2 for different angles $\theta$. The figure is valid for any Poisson's ratio, which is not the case for standard finite-difference schemes. The quantity $q_p$ is always lower than 1 and approaches 1 for small $H$. For $H \simeq 0.1$, $q_p \simeq 1$. This is the rule of thumb stating that ten nodes are needed inside a wavelength for correct modeling. For $\gamma = 0.8$, $q_s(H)$ is shown on Figure 3 for different angles $\theta$ and for different Poisson's ratios $\nu$. The quantity $q_s$ is always lower than 1. This is not the case for usual finite-difference schemes where $q_s$ may be found to be higher than 1 (Bamberger et al., 1980), which means that the numerical-$S$-wave propagates faster than the true $S$-wave. The quantity $q_s$ approaches 1 for small $H$, giving the same rule of thumb as for the $P$-wave modeling. Because the $S$-wave velocity is lower than the $P$-wave velocity, the condition on the $S$-wave is more restrictive and will overrule the one on the $P$-wave. Moreover, the behavior of $q_s$ does not degrade as $\nu$ goes to 0.5, while $q_s$ becomes infinite inside liquids for standard finite-difference schemes (Bamberger et al., 1980). This suggests, as is confirmed later, that our numerical scheme behaves correctly inside liquids, and at liquid-solid interfaces.

Finally, for a medium of size $400 \times 200$, a computer memory of $850\ K$ words is needed. 100 s are necessary to perform 1 200 time steps on a CRAY 1-S. Although the numerical code was designed to handle any size of medium by using its own virtual memory, this option was not used because it increases drastically the I/O computing cost.

### COMPARISON WITH ANALYTICAL RESULTS

Two problems arise in the modeling of $P$-$SV$ wave propagation which require a numerical solution. These are source modeling and surface wave (Rayleigh wave) modeling. These features are not simple extensions from the $SH$-wave case, and need to be checked with simple analytical solutions.

### Explosive source

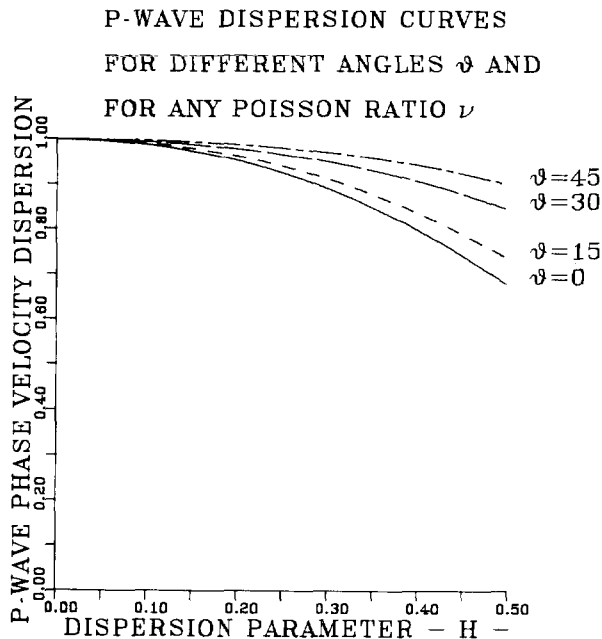Although any kind of source may be implemented, an explosive source is easily modeled by adding a known value to

stress ($\tau_{xx}$, $\tau_{zz}$) at the point source. A point force at the free surface of a half-space is modeled incrementing only $\tau_{zz}$ at this point source.

For a source excitation $g(t)$ given by equation (4) with a parameter $\alpha$ equal to 40, I compared the radial numerical displacement with the analytical solution in an infinite medium of *P*-wave velocity equal to 4 000 m/s. Figure 4 pictures the seismogram at a station 400 m from the source. The tangential displacement, which is not zero because of numerical dispersion, remains negligible. Its amplitude decreases when the parameter $\gamma$ diminishes or when the spectral content of the source shifts to lower frequencies.

### Lamb's problem

Rayleigh surface waves are strongly excited by a source at the free surface of a half-space. Since the work of Lamb (1904), analytical solutions have been presented in many textbooks (Ewing et al., 1957; Aki and Richards, 1980). The Cagniard-De Hoop method is an elegant way of computing body wave seismograms (Achenbach, 1975, p. 303). Moreover, the Cagniard path is known analytically for a source at the free surface. A difficulty arises when the station is also at the free surface. The Rayleigh pole in the complex slowness plane is located on the Cagniard path: its contribution must be evaluated by the theorem of residues (Ben-menahem and Singh, 1981, p. 545). The seismogram for any source excitation is obtained by convolution of the solution for Dirac's $\delta$ pulse with the source time function.

Figure 5, shows the horizontal component due to a vertical Gaussian point source $f(t)$ of the type (3), with a spectral

parameter $\alpha = 200$. Observe the propagation without dispersion of the surface wave and the build-up of the conical wave. The numerical Rayleigh wave has a lower amplitude than does the analytical Rayleigh wave. This slight misfit, which is the same for $X = 1\ 500$ m or $X = 3\ 000$ m, does not depend on the propagation and may be explained by the discretization of the medium at the source. At early times, interaction between the source and the free surface involves a few nodes. Because the propagation is correctly modeled, I consider that the agreement between numerical and analytical solutions is satisfactory.

### COMPARISON WITH NUMERICAL RESULTS

For more complex models of the medium, only numerical solutions are available for comparison. Two models are presented: the weathered-layer model for Rayleigh wave excitation by a point source at depth, and the corner-edge model for diffraction. These models were chosen because they present more complex wave patterns than do the analytical solutions and because they have been studied by Kelly et al. (1976) which makes qualitative comparison achievable.

### Weathered-layer model

The geometry of the medium is shown in Figure 6. The upper layer has a very low *P*-wave velocity of 2 000 m/s compared to the velocity of the half-space which is 6 000 m/s. Density is taken as a constant of 2 500 kg/m³. The source $g(t)$, with a spectral content defined by $\alpha = 40$, see equation (4), is
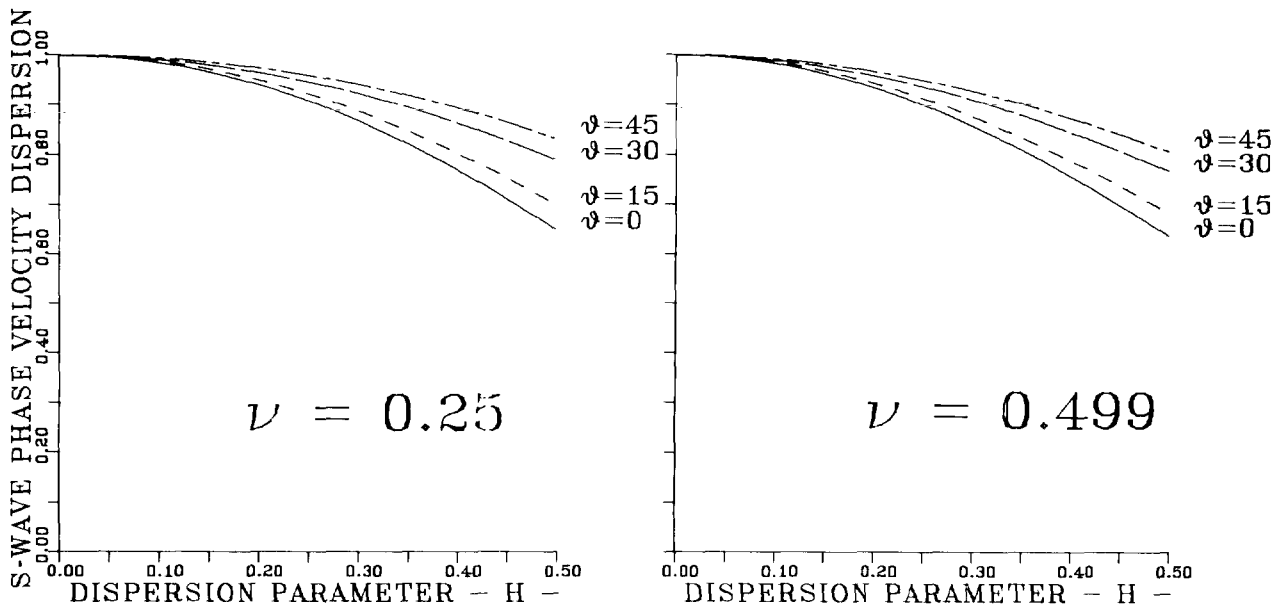


FIG. 3. Dispersion curves for nondimensional *S*-wave phase velocity with a dispersion parameter $\gamma = 0.8$. Results for different angles $\theta$ of the plane wave with respect to the *x*-axis are shown on the same graph for different Poisson's ratios $v$.

located near the surface in order to obtain efficient Rayleigh wave excitation. In Figure 7, seismograms lasting 5 s present the features already studied in Kelly et al. (1976). A quantitative comparison is difficult because of the unknown spectral source content of Kelly et al. (1976) and because of the graphical representation of seismograms. The direct P-wave and the Rayleigh wave dominate the seismograms. The PP- and PS-wave reflections clearly show a phase shift after the critical angle. The reflection at the free surface, which seems to come from a ghost source above the free surface, is called GP for the P-wave reflection and GS for the S-wave reflection. These phases are usually called pP and sP but I use the nomenclature of Kelly et al. The GP phase is again reflected upward by the interface as a P-wave. This so-called GPP phase stands between the PP and PS reflection. The head wave can be guessed, mainly when it arrives before the direct P-wave. With another choice of saturation for the picture, it would have been clearly seen. Then, the S reflection of GP phase, called GPS, and the P reflection of GS phase, called GSP, arrive in front of the phase obviously called GSS. The PPPP phase, which is the P incident phase twice reflected at the interface and once at the free surface, can hardly be seen at the bottom of the seismogram.

I now show raster pictures instead of the more conventional representation in Figure 7. Small energetic phases are better seen on raster images.

### Corner-edge model

This model is a stringent test for the quality of a finite-difference scheme. Kelly et al. (1976) showed unacceptable discrepancies between the solutions obtained with the homogeneous and heterogeneous formulations of the problem.

The geometry of the medium is shown in Figure 8. The velocity of the upper medium is 6 000 m/s while the lower medium has a velocity of 9 000 m/s. The density of the lower medium is 2 500 kg/m$^3$. The source $g(t)$ has a spectral content
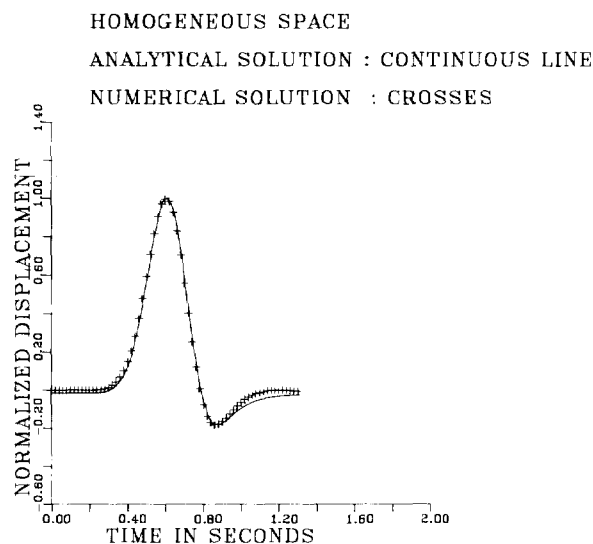
HOMOGENEOUS SPACE

ANALYTICAL SOLUTION : CONTINUOUS LINE

NUMERICAL SOLUTION : CROSSES



FIG. 4. Comparison between numerical and analytical seismograms for an explosive source in an infinite medium.

HALF-SPACE VELOCITY Vp = 4 000 M/S

CAGNIARD-DE HOOP   CONTINUOUS LINE
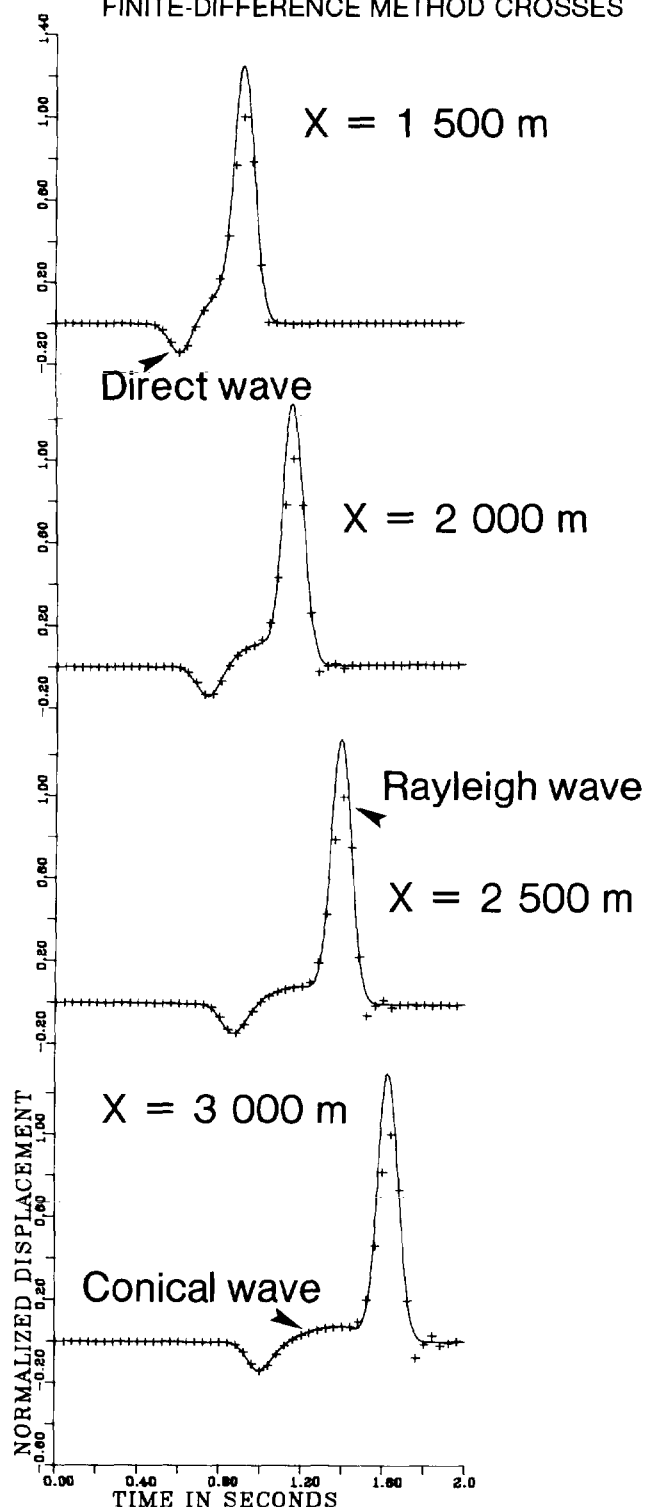
FINITE-DIFFERENCE METHOD CROSSES



FIG. 5. Comparison between numerical and analytical horizontal components for Lamb's problem at different stations on the free surface.

defined by $\alpha = 40$, [see equation (4)]. Figure 9 presents seismograms lasting 6 s on the free surface for $\Delta x = \Delta z = 100$ m. Two models were considered: (1) homogeneous density, where the two media have the same density, and (2) homogeneous Lamé coefficients, where the two media have the same $\lambda$ and $\mu$. They illustrate the phase shifts for the different waves at the interface. Time arrivals of numerical waves are compared with those obtained by ray tracing. I use the same nomenclature of phases used in the previous example. After the direct *P*-wave, the $PP_{\text{refl}}$ reflection is associated with the $PP_{\text{diff}}$ diffraction. The $PS_{\text{refl}}$ is clearly seen on the horizontal component, but interferes later with the ghost $GPP_{\text{refl}}$ reflection and the ghost $GPP_{\text{diff}}$ diffraction, which are strong above the corner and source area. Another group of energetic waves, *GPS* and *GSP* waves, which are the *S*-wave reflection of the *GP* phase at the interface or the *P*-wave reflection of the *GS* phase, are not hidden by the residual reflection coming from the bottom where numerical radiation conditions were applied. Kelly et al. (1976) mainly observed this reflection because they did not apply absorbing radiation conditions.

These different phases may be followed by snapshots of the medium at successive times. Figure 10 shows the horizontal and vertical components. Wavefronts are indicated with arrows. Attention must be drawn on diffracted fronts, head fronts, and corner fronts. The corner front is the same one observed for the *SH* case (Virieux, 1984). This front, called C phase in Figure 10, corresponds to the *P*-wave refracted on the horizontal interface, and reflected again on the vertical wall as an *S* wave.
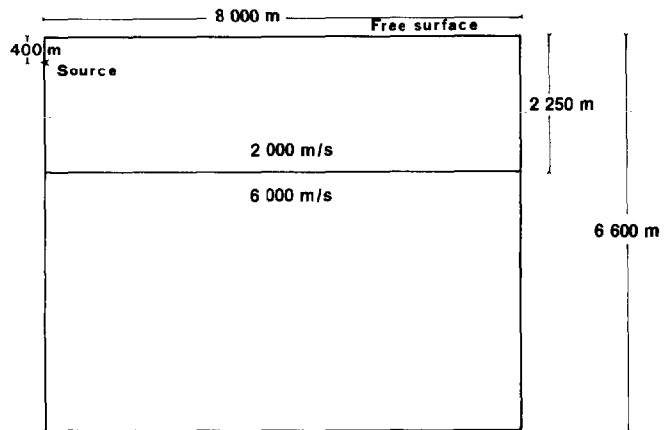


FIG. 6. Geometry of the weathered-layer model.
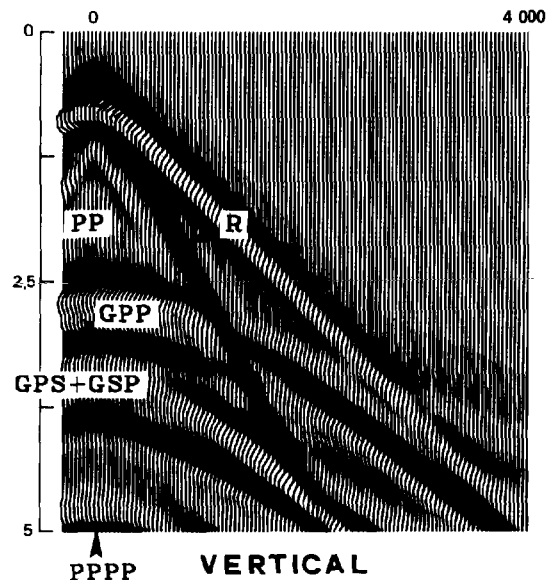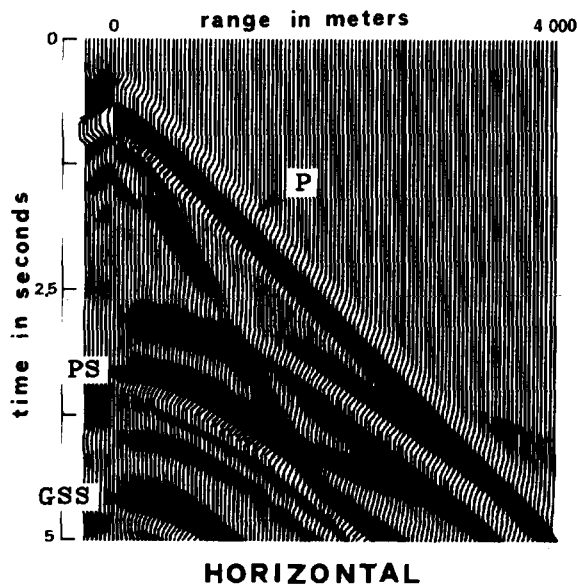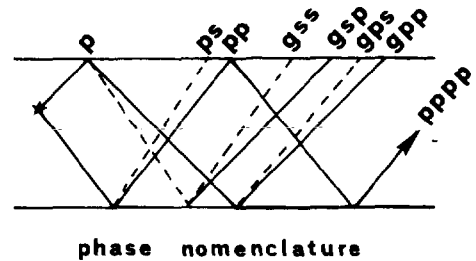


phase nomenclature



FIG. 7. Numerical seismograms at the free surface for the weathered-layer model. The horizontal seismogram is shown on the left and the vertical seismogram is shown on the right. Phases are indicated by arrows following the ray nomenclature given in the upper right corner.

Returning to the discrepancy between the homogeneous and heterogeneous formulations of finite-differences at interfaces, Kelly et al. (1976) argue that a possible explanation may come from the numerical smoothing of Lamé coefficients in the heterogeneous formulation. There is a numerical transition zone which is not found in the homogeneous formulation because of the explicit boundary conditions. With the increasing power of computers this argument may be reexamined by numerical scaling. By decreasing the grid size, the transition zone is reduced, and results for the heterogeneous formulation are expected to improve. This is not the case. Taking $\Delta x = 200$ m, $\Delta x = 100$ m and $\Delta x = 50$ m, results are remarkably stable and give a very weak $PS$ diffracted signal in the forward direction compared with that in the backward direction. This signal is not as strong as that found by the homogeneous formulation of Kelly et al. (1976) and the result confirms numerically Gupta's results (Gupta, 1966) on analytical transition zones. A source with a wavelength content between 10 and 20 nodes cannot distinguish drastically a transition zone over 1, 2, or 3 nodes from an abrupt change of physical parameters because the source does not have enough resolution. Therefore, another explanation may be sought. I give two arguments for a weak $PS$ diffraction.

The energy of the incident wave is divided in two parts at a plane interface: the reflected part, going upward and the refracted part, going downward. The diffraction phase, which comes from an abrupt end of the interface, connects the upward reflected phase to the downward incident phase. The incident phase, where the interface is missing, is stronger than the refracted phase. Therefore, only a small amount of energy is expected to go upward with the diffracted front, while the incident phase brings downward the main part of the energy.

A possible analytical way is to look at asymptotic solutions in the high-frequency approximation. I could compare numerical solutions for a high-frequency source with solutions obtained by the geometrical theory of diffraction (Keller, 1962) applied to elastic waves. Instead, I argue qualitatively from results presented in Achenbach et al. (1982). The corner-edge model is not too different from the semiinfinite crack diffraction problem. The contribution of the vertical wall of the corner is missing, but the contribution from the interruption of the horizontal wall is expected to be correctly modeled. Illuminating the horizontal wall by a compressional plane wave making an angle $\theta_1$ with the $x$-axis, Achenbach et al. (1982, p. 126-148) obtained $PS$ diffraction coefficients. For any angle $\theta_1$ between 0 and $\pi/2$ of this plane wave, the amplitude was an order of magnitude smaller in the forward direction than in the backward direction.
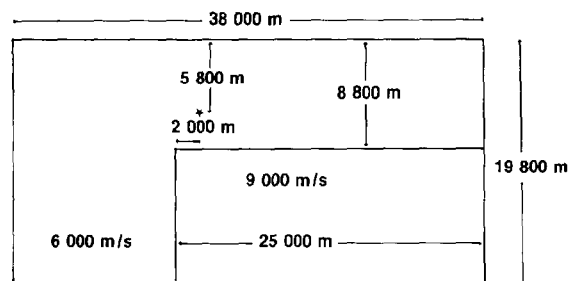
As a partial conclusion, the heterogeneous formulation of Kelly et al. (1976) or the heterogeneous formulation of this article present reasonable solutions while the homogeneous formulation of Kelly et al. (1976) presents features difficult to explain. For a more precise analysis the computer program used by Kelly et al. for the homogeneous formulation is needed.

## LIQUID OVER SOLID INTERFACE: CORNER-EDGE MODEL

Interest in the liquid-solid interface increases with marine seismic exploration. Waves propagate inside water before hitting the ocean basement and penetrating an elastic medium. Does the problem require a new formulation?

The heterogeneous formulation of standard finite-difference schemes exhibits instabilities for step discontinuities at a liquid/solid interface or inaccuracies for gradient discontinuities, as clearly shown in Stephen (1983). Solving this problem requires the homogeneous formulation of finite-difference schemes. Propagation inside water is solved by the acoustic equation, while the propagation inside an elastic medium is solved by the elastodynamic equations. The liquid-solid interface is a common boundary. Different approximations used at this interface yield different numerical schemes. Modeling complex interfaces with a homogeneous formulation is a difficult computational task, and has not yet been performed, to my knowledge.

I illustrate the liquid-solid interface with two models: the 2-D step discontinuity model for showing stable results, and the corner-edge model for analyzing the complex liquid/solid interface.

### Step-discontinuity model

Stephen (1983) studied the same problem but used cylindrical symmetry to simulate point sources. He found unstable results for a step discontinuity of velocity and density with depth, using a heterogeneous formulation. This instability does not come from the cylindrical symmetry of his problem, but results from the numerical feature of the standard finite-difference scheme he used. Figure 11 presents results for the same medium, using my heterogeneous formulation which gives stable results. Unfortunately, comparison with Stephen's results is not possible because my flat 2-D geometry is different from his cylindrical calculations. My results exhibit reasonable amplitudes at any range and a good modeling of conical phases at supercritical (4 000 m) range.

### Corner-edge model

Now consider the corner-edge model presented previously. Figure 12 presents seismograms for the same medium as Figure 9, but for different Poisson's ratios ranging from 0.25 to 0.5. The pattern for the direct $P$-wave and the $PP$-wave remains essentially the same for the different Poisson's ratios, while the $PS$-wave moves downward because the $S$-wave velocity decreases and then disappears completely for the Poisson's ratio $v = 0.5$. Small oscillations coming from the $S$-wave generated by the free surface may be observed when the number of nodes inside the $S$ wavelength is too small. For this scheme, they go to zero when $v$ tends toward 0.5.

A better understanding of these seismograms may be obtained from the snapshots of the medium for different Pois-



Fig. 8. The geometry of the corner-edge model.

HORIZONTAL COMPONENT VERTICAL COMPONENT
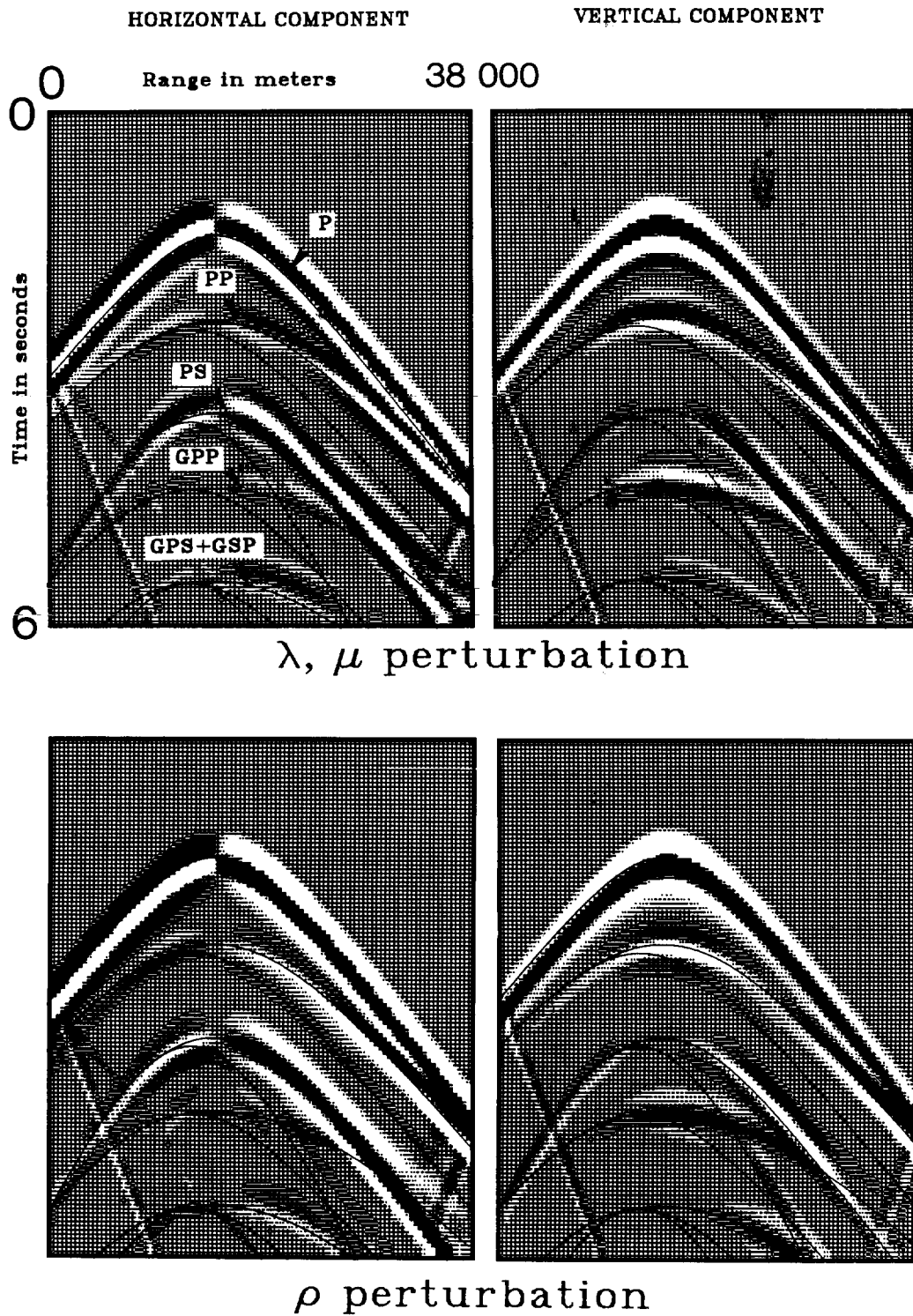


λ, μ perturbation



ρ perturbation

FIG. 9. Numerical seismograms at the free surface for the corner-edge model. The horizontal seismogram is shown on the left and the vertical seismogram is shown on the right. Continuous lines are arrival times of different waves from ray tracing.
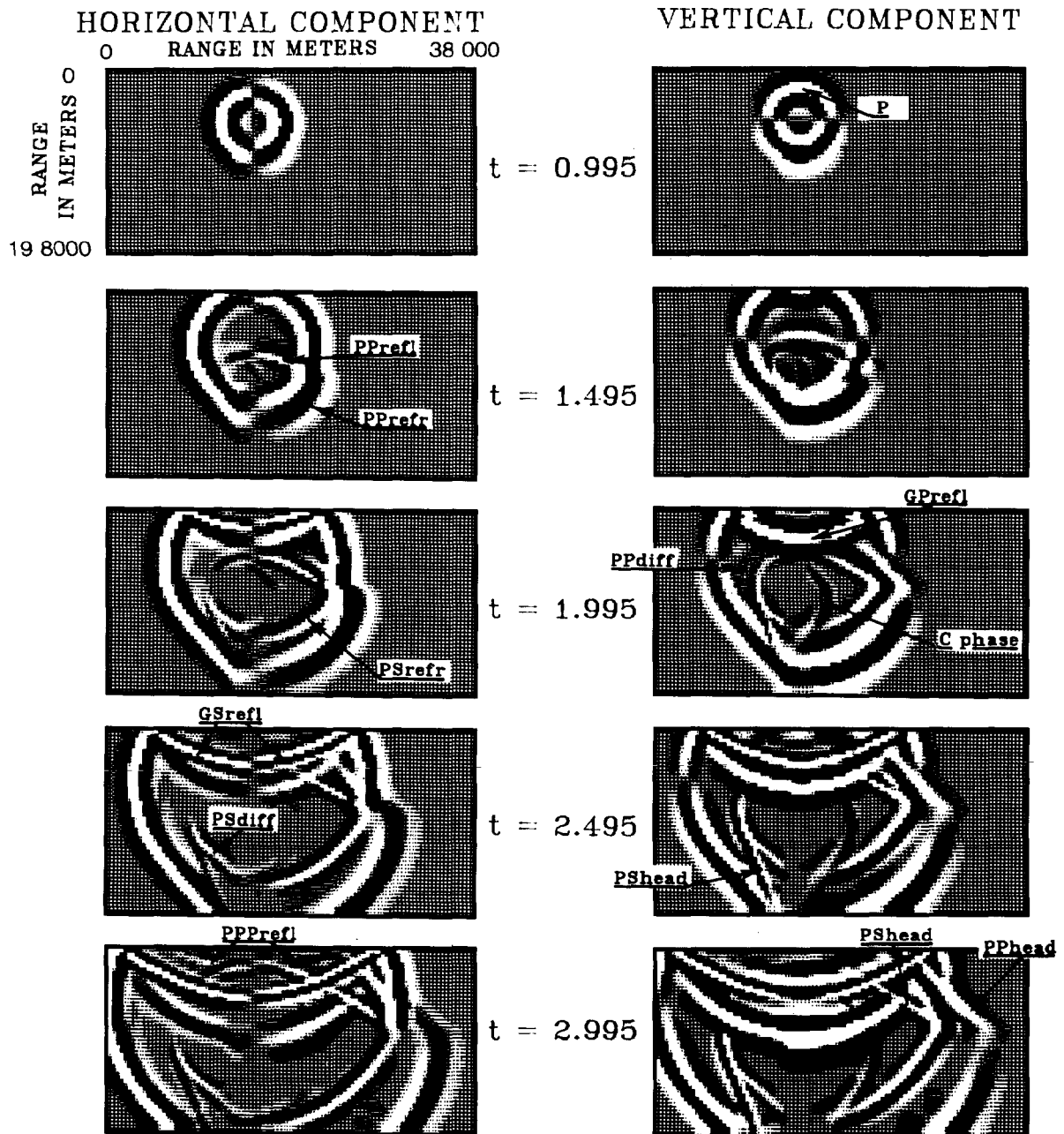
HORIZONTAL COMPONENT

VERTICAL COMPONENT

0 RANGE IN METERS 38 000

RANGE IN METERS

0

19 8000

t = 0.995

t = 1.495

t = 1.995

t = 2.495

t = 2.995

P

PPrefl

PPrefr

GPrefl

PPdiff

C phase

PSrefr

GSrefl

PSdiff

PShead

PPPrefl

PShead

PPhead

FIG. 10. Pictures of the corner-edge medium for different times. Wavefronts are indicated by arrows.

son's ratios v. Figure 13 shows vertical component at time $t = 2.995$ s inside the medium. To observe the modification of the wave pattern, look at the *PS* reflection/diffraction on the corner edge. As the Poisson's ratio tends toward 0.5, the *PS* wavefront becomes increasingly confined near the interface. Another modification comes from the free surface. The *PS* reflection at the free surface precedes slightly the *GPP* reflection for v = 0.25. For v = 0.45, the *PS* reflection is behind the *GPP* reflection, while, for greater v, the *PS* is unnoticeable and disappears for v = 0.5.

Stable and accurate results were obtained in Nicoletis (1981) at a liquid-solid interface. Using variational methods, she designed a numerical scheme for the acoustic problem inside the liquid and another scheme for the elastic problem inside the solid with an explicit boundary between them. In our technique, it is not necessary to use an explicit boundary condition between the solid and liquid. The same unique numerical scheme is applied to the liquid and solid media. Therefore, propagation of elastic waves and acoustic waves across a liquid-solid interface is modeled with the same code. No special treatment of the interfaces is needed to allow our method to model complex geometries of the interfaces.

## CONCLUSION

I have shown that elastodynamic equations can be solved by a finite-difference technique using velocity and stress as conjugate physical quantities distributed on a staggered grid. The numerical solution is valid for any Poisson's ratio. Liquid areas can be introduced inside the heterogeneous medium and the wave equation can be solved using the same formulation used for a solid, thereby avoiding use of the acoustic equation inside the liquid and escaping the rather complex problem of connecting the liquid and solid areas along an interface.

The main limitations of our stress-velocity finite-difference method come from the numerical dispersion and the finite numerical size of the grid. With these restrictions, interpretation of numerical seismograms may be very difficult for complex media. By choosing different hypothetical media, differential seismograms may be built to analyze where the energy is coming from. Ray theory and its extension may also be used to locate different phases. These different methods are essential for understanding wave propagation in a complex medium (George et al. 1985).

Another alternative to this trial-and-error method consists of applying inverse techniques to the nonlinear problem. Techniques are currently being developed using this stress-velocity formulation (Gauthier et al., 1985).
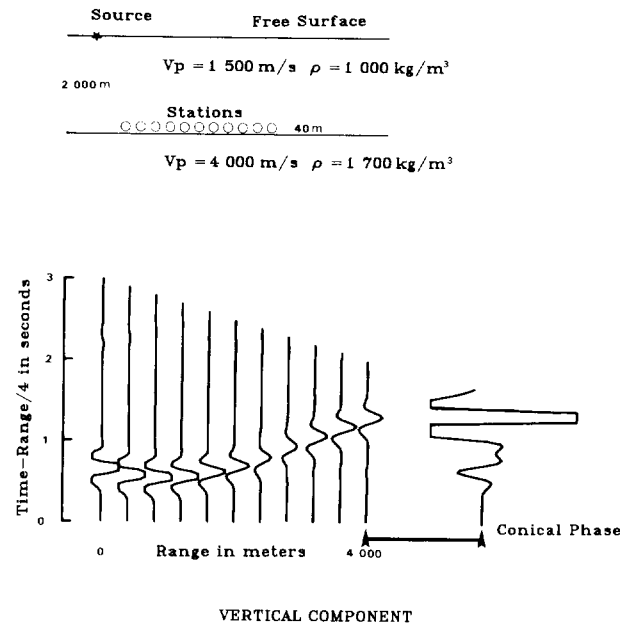
## ACKNOWLEDGMENTS

FIG 11. Numerical vertical seismograms above the interface between liquid and solid media, as depicted in the upper left. The seismogram at offset 4 000 m is amplified in order to see the conical phase propagating at 4 000 m/s.

## REFERENCES

Achenbach, J. D., 1975, Wave propagation in elastic solids: North Holland Publ. Co.
Achenbach, J. D., Gautesen, A. K., and McMaken, H., 1982, Ray methods for waves in elastic solids: Pitman Publ. Inc.
Aki, K., and Larner, K. L., 1970, Surface motion of a layered medium having an irregular interface due to incident plane *SH*-waves: J. Geophys. Res., **75**, 933–954.
Aki, K., and Richards, P., 1980, Quantitative seismology, theory and methods: W. H. Freeman & Co.
Alekseev, A. S., and Mikhailenko, B. G., 1980, The solution of dynamic problems of elastic wave propagation in inhomogeneous media by a combination of partial separation of variables and finite-difference methods: J. Geophys., **48**, 161–172.
Alterman, Z., and Karal, F. C., 1968, Propagation of elastic waves in layered media by finite-difference methods: Bull. Seism. Soc. Am., **58**, 367–398.
Bamberger, A., Chavent, G., and Lailly, P., 1980, Etude de schémas numériques pour les équations de l'élastodynamique linéaire: Rapports de recherche **41**, INRIA.
Bard, P. Y., and Bouchon, M., 1980, The seismic response of sediment-filled valleys. Part 1: The case of incident *SH* waves: Bull. Seism. Soc. Am., **70**, 1263–1286.
Ben-menahem, A., and Singh, S. J., 1981, Seismic waves and sources: Springer-Verlag New York Inc.
Boore, D. M., 1972, Finite-difference methods for seismic wave propagation in heterogeneous materials, in Bolt, B. A. Ed., Methods in computational physics, **11**: Academic Press, Inc.
Červený, V. Molotkov, I. A., and Pšenčik, I., 1977, Ray method in seismology: Univ. of Karlova.
Chapman C. H., 1978, A new method for computing synthetic seismograms: Geophys. J. Roy. Astr. Soc., **64**, 321–372.
Chapman, C. H., and Drummond, R., 1982, Body-wave seismograms in inhomogeneous media using Maslov asymptotic theory: Bull. Seism. Soc. Am., **72**, 5277–5317.

Clayton, R. W., and Engquist, B., 1980, Absorbing boundary conditions for wave-equation migration: Geophysics, **45**, 895–904.

Ewing, W. M., Jardetzky, W. S., and Press, F., 1957, Elastic waves in layered media: McGraw-Hill Book Co.

Fuchs, K., and Müller, G., 1971, Computation of synthetic seismograms with the reflectivity method and comparison with observations: Geophys. J. Roy. Astr. Soc., **23**, 417–433.

Gauthier, O., 1983, Inversion de données de sismique réflexion dans l'approximation acoustique: Rapport de stage de D.E.A., Univ. de PARIS 7.

Gauthier, O., Virieux, J., and Tarantola, A., 1985, Two-dimensional non-linear inversion of seismic waveforms: numerical results in press.

George, T., Virieux, J., and Madariaga, R., 1985, Gaussian beam of complex structures: comparison with other techniques in press.

Gupta, R. N., 1966, Reflection of elastic waves from a linear transition layer: Bull. Seism. Soc. Am., **56**, 511–526.

Helmberger, D. V., 1968, The crust-mantle transition in the Bering Sea: Bull. Seism. Soc. Am., **58**, 179–214.

Hong, T. L., and Helmberger, D. V., 1978, Glorified optics and wave propagation in nonplanar structure: Bull. Seism. Soc. Am., **68**, 2013–2032.

Keller, J. B., 1962, Geometrical theory of diffraction: J. Opt. Soc. Am., **52**, 116–130.

Kelly, K. R., Ward, R. W., Treitel, S., and Alford, R. M., 1976, Synthetic seismograms: A finite-difference approach: Geophysics, **41**, 2–27.
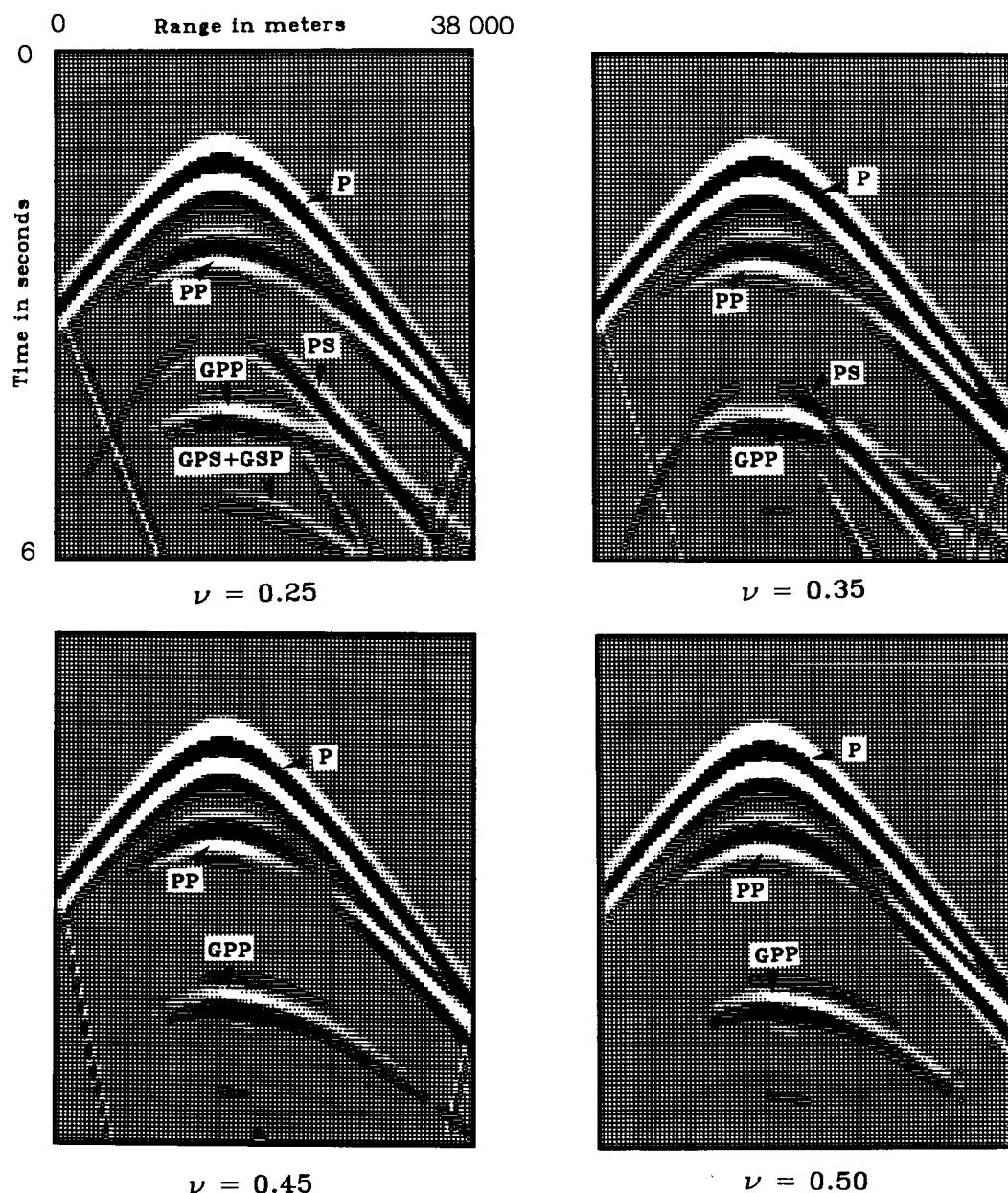
# VERTICAL COMPONENT



FIG. 12. Evolution of vertical numerical seismograms from the solid-solid corner-edge model to the liquid-solid corner-edge model. Different Poisson's ratios v are taken for 0.25 to 0.5.

Lamb, H., 1904, On the propagation of tremors over the surface of an elastic solid: Phil. Trans. Roy. Soc. London., **A203**, 1–42.

Lee, J. J., and Langston, C. A., 1983, Three-dimensional ray tracing and the method of principal curvature for geometric spreading: Bull. Seism. Soc. Am., **73**, 765–780.

Madariaga, R., 1976, Dynamics of an expanding circular fault: Bull. Seism. Soc. Am., **66**, 163–182.

Madariaga, R., and Papadimitriou, P., 1985, Gaussian beam modelling of upper mantle phases: Annal. Geophys., in press.

Marchuk, G. I., 1975, Methods of numerical mathematics: Springer-Verlag New York, Inc.

Mikhailenko, B. G., and Korneev, V. I., 1984, Calculation of synthetic seismograms for complex subsurface geometries by a combination of finite integral Fourier transforms and finite difference techniques: J. Geophys., **54**, 195–206.

Nicoletis, L., 1981, Simulation numérique de la propagation d'ondes sismiques dans les milieux stratifiés à deux et trois dimensions: contribution à la construction et à l'interprétation des sismogrammes synthétiques: Thèse, Univ. Pierre et Marie Curie.

Smith, W. D., 1975, The application of finite-element analysis to body wave propagation problems: Geophys. J. Roy. Astr. Soc., **42**, 747–768.

Stephen, R. A., 1983, A comparison of finite difference and reflectivity seismograms for marine models: Geophys. J. Roy. Astr. Soc., **72**, 39–58.

Virieux, J., 1984, *SH*-wave propagation in heterogeneous media: Velocity-stress finite-difference method: Geophysics, **49**, 1933–1957.

Virieux, J., and Madariaga, R., 1982, Dynamic faulting studied by a finite difference method: Bull. Seism. Soc. Am., **72**, 345–369.

Zienkiewicz, O. C., and Morgan, K., 1982, Finite elements and approximation: John Wiley & Sons, Inc.
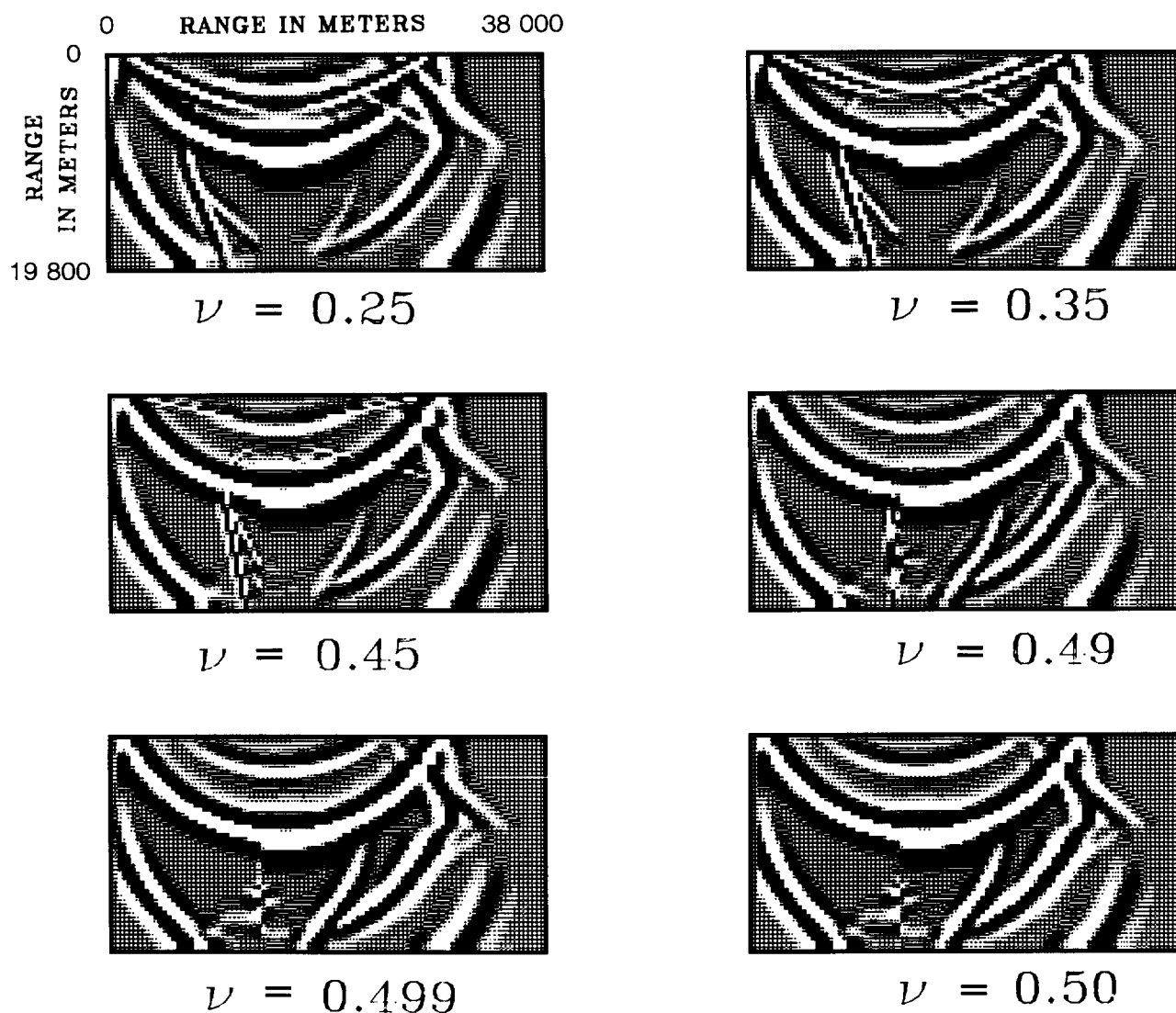
# VERTICAL COMPONENT



FIG. 13. Pictures of the corner-edge medium for different Poisson's ratios at the same time $t = 2.995$ s. See figure 10 for the wavefront interpretation.